Supporting Information for

Ag_2S-gated ion rectification in confined AgNCs@UiO-66 nanochannels enables sensitive monitoring of bacterial H_2S release

Xiaotong Cui[a,b,‡], Yuxin Xie[a,b,‡], Siyu Wan[a,b], Zhonggang Liu[a,b,*], Zheng Guo[a,b,*], Xingjiu Huang[a,c]

[a] State Key Laboratory of Opto-Electronic Information Acquisition and Protection Technology, Institutes of Physical Science and Information Technology, Anhui University, Hefei, 230601, P.R. China

[b] Key Laboratory of Structure and Functional Regulation of Hybrid Materials of Ministry of Education, Anhui University, Hefei, 230601, P.R. China

[c] Key Laboratory of Environmental Optics and Technology, and Environmental Materials and Pollution Control Laboratory, Institute of Solid State Physics, HFIPS, Chinese Academy of Sciences, Hefei, 230031, P.R. China

[‡]These authors contributed equally to this work.

**Corresponding author:*

E-mail: zhgliu@ahu.edu.cn (Z. Liu), zhguo@ahu.edu.cn (Z. Guo)

S1. Methods

S1.1. Chemicals

All chemicals were used directly without further purification. Zirconium tetrachloride ($ZrCl_4$), 1,4-dicarboxybenzene (H_2BDC), acetic Acid (HAc, 99.5%), dopamine (DA), silver nitrate ($AgNO_3$), sodium sulfide (Na_2S), sodium Chloride (NaCl), cysteine (Cys), glutathione (GSH), hydrogen peroxide (H_2O_2), L(+)-ascorbic acid (AA), uric acid (UA), serotonin (5-HT), ammonium chloride (NH_4Cl), tris (hydroxymethyl) aminomethane (Tris), glycerin ($C_3H_8O_3$), glycerol, N,N-dimethylformamide (DMF), were purchased from Macklin. Deionized water (18.2 MΩ cm at 25ºC) was used throughout this work. Platinum wire (0.025 mm diameter, 99.99%, Goodfellow, U.K.). Unless stated otherwise, all experiments were carried out at room temperature.

S1.2. Synthesis of UiO-66(Zr)

UiO-66(Zr) was prepared based on the previous report with slight modifications [1]. Briefly, 0.4 mmol $ZrCl_4$ and 0.4 mmol H_2BDC, and 28 mmol HAc were successively dissolved in 28 mL DMF. The resulting solution was transferred to a 50 mL Teflon-lined auto-clave and heated at 120°C for 24 h. Then, the obtained mixture was centrifuged and washed several times with DMF and methanol. Thereafter, the product was dried under vacuum at 60°C for 18 h for further characterization and measurements.

S1.3. Synthesis of AgNCs@UiO-66

Initially, 20 mg UiO-66(Zr) was uniformly dispersed in 8 mL of deionized water, and the aqueous solution of DA (0.1 mg mL^{-1}, 8 mL) was slowly added under continuous stirring for 90 min. After that, the DA modified UiO-66 was obtained by centrifugation and washed with deionized water. The DA modified UiO-66 was re-dispersed in 8 mL of water, and 4 mL $AgNO_3$ solution (0.1 mg mL^{-1}) was added dropwise in the above solution. The mixture solution was stirred at room temperature for about 7 h to allow for the reduction and deposition of Ag nanoclusters (AgNCs). Subsequently, a grey precipitate was separated by centrifugation at 9000 rpm for 5 min. Finally, the product was dried under vacuum at 60°C for 18 h for further

application.

S1.4. Material characterization

The morphology and structure of the prepared AgNCs@UiO-66 were characterized using field emission scanning electron microscopy (FE-SEM, 15 kV Quanta 200 FEG, FEI Company, USA), and transmission electron microscopy (TEM, JEOL-2010). The crystalline structure was characterized using X-ray diffraction (XRD, Smart Lab 9 KW) with Cu Ka radiation. X-ray photoelectron spectroscopy (XPS, VERTEX 80, Thermoelectric company, USA) was applied to analyze element composition and chemical state. The structural characteristics were determined by using the ASAP 2460 3.01e instrument to perform N_2 adsorption-desorption isotherms at a temperature of 77.3 k. Fourier transform infrared spectroscopy (FT-IR) tests were performed on a Hyperion 2000 FT-IR spectrometer. Zeta potential measurements were acquired on a zeta potential analyzer (NanoBrook 90plus PALS, Brookhaven Instruments, U.S.A).

S1.5. Fabrication of modified nanopipette

Glass nanopipettes were constructed using quartz capillaries with an outer diameter of 1.0 mm and an inner diameter of 0.7 mm (QF100-70-10, Sutter Instrument, Novato, CA). Firstly, the capillaries were treated with a piranha solution for 4 h (*a mixture of 98% sulfuric acid and 30% hydrogen peroxide in a 3:1 volume ratio, caution: It is imperative to note that piranha solution is highly reactive with organic substances and can become dangerously hot during preparation.*). After that, the capillaries were extensively rinsed with distilled water and acetone. The nanopipettes were pulled using a CO_2 laser puller (P-2000, Sutter Instrument, Novato, CA) in the following parameters: HEAT = 700; Fil = 3; VEL = 40; DEL = 175, and PULL = 190. Then the glass nanopipette with a sharp tip was grinded using micro grinder (EG-402, NARISHIGE) to obtain a tip diameter of 30 μm. AgNCs@UiO-66 was uniformly ultrasonically dispersed in deionized water (5 wt %, 1.0 mL). The above dispersion was injected into the nanopipette and kept overnight to dry.

S1.6. Electrochemical measurements

Before the measurement, the AgNCs@UiO-66/micropipette was back-filled with 0.1

M NaCl solution. The electrochemical measurements were performed in a two-electrode system using an AutoLab potentiostat (PGSTAT302N, Metrohm, Germany). In a two-electrode system, an AgNCs@UiO-66/micropipette with a platinum wire inserted inside was served as the indicator electrode, and a platinum wire was applied as the counter electrode and reference electrode, in which 0.1 M NaCl solution was used as the electrolyte. All potentials were referenced against the Pt electrode. It was conducted in a voltage window between +1.0 V and -1.0 V with a scan rate of 50 mV s^{-1}. The current values at -1.0 V were measured and recorded.

S2. Characterization of AgNCs@UiO-66(Zr)

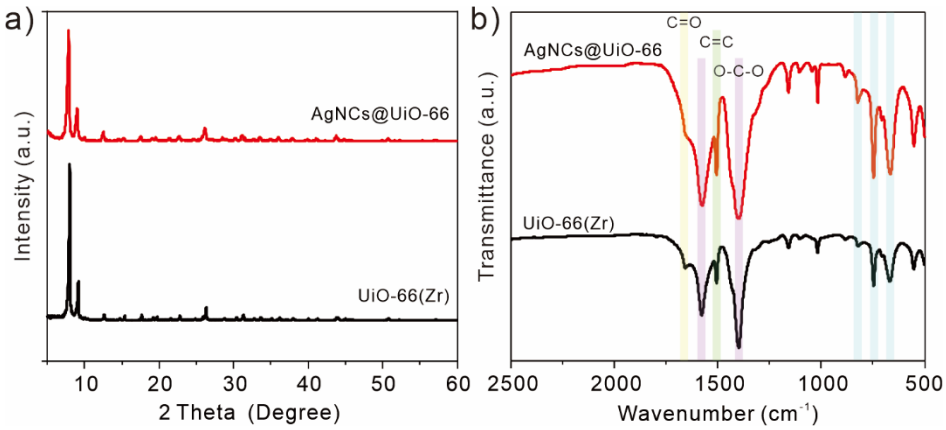

Fig. S1. (a) XRD patterns and (b) FT-IR spectra of UiO-66(Zr) and AgNCs@UiO-66(Zr).

The characteristics bands for UiO-66(Zr) and AgNCs@UiO-66 can be clearly observed through Fourier transform infrared spectroscopy (FTIR) (Fig. S1b). The weak absorption band at 1660 cm^{-1} corresponds to the stretching vibrations of the C=O bond in the carboxylic acid moiety of BDC. The characteristic bands at 1580 cm^{-1} and 1399 cm^{-1} are attributed to the asymmetric O-C-O stretching and symmetrical O-C-O stretching within BDC. The band at 1506 cm^{-1} is related to the vibrations in the C=C bonds of benzene rings. Furthermore, the bands observed at 825, 746 and 668 cm^{-1} are attributed to the vibrations of the OH and C-H groups in the BDC ligand [2].

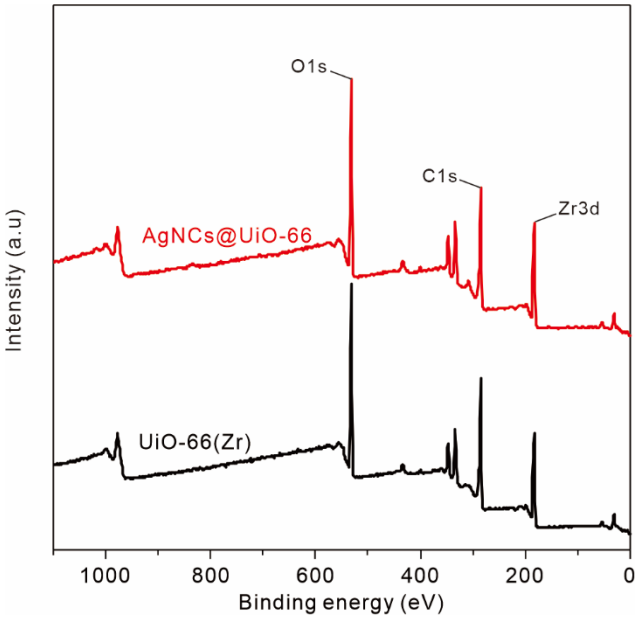

Fig. S2. Full scan XPS spectra of UiO-66(Zr) and AgNCs@UiO-66(Zr).

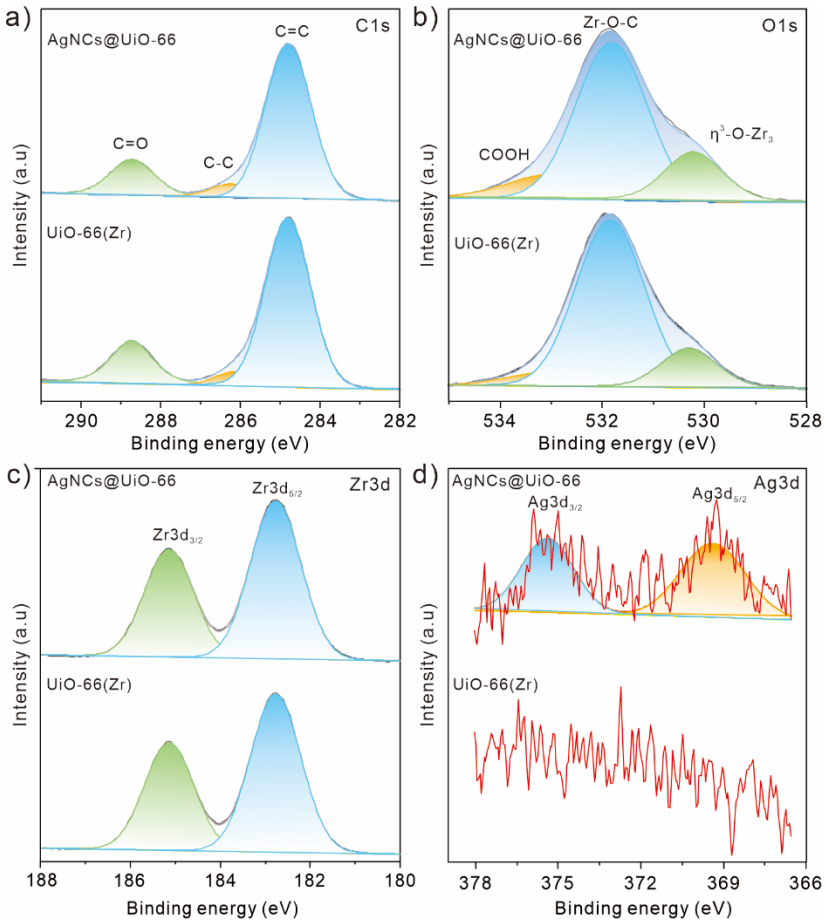

Fig. S3. High resolution XPS spectra of (a) C 1s, (b) O 1s, (c) Zr 3d, (d) Ag 3d in UiO-66(Zr) and AgNCs@UiO-66(Zr).

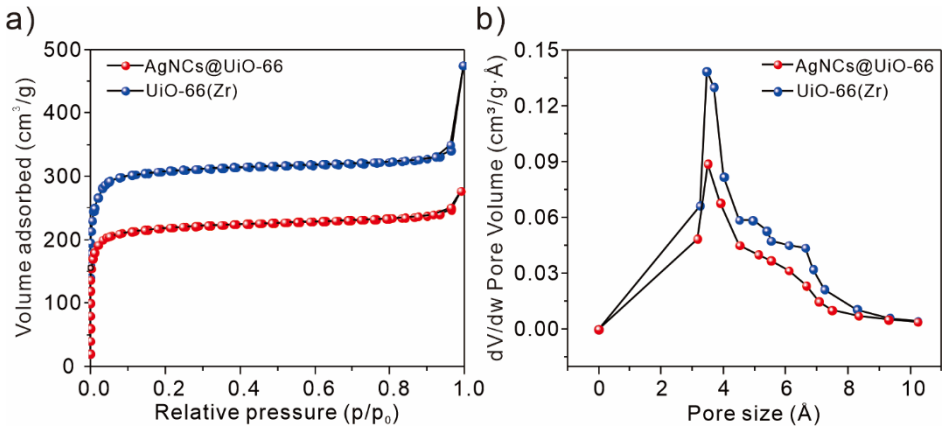

Fig. S4. (a) N_2 adsorption/desorption isotherms and (b) pore size distributions of UiO-66(Zr) and AgNCs@UiO-66.

S3. Micropipette characterization

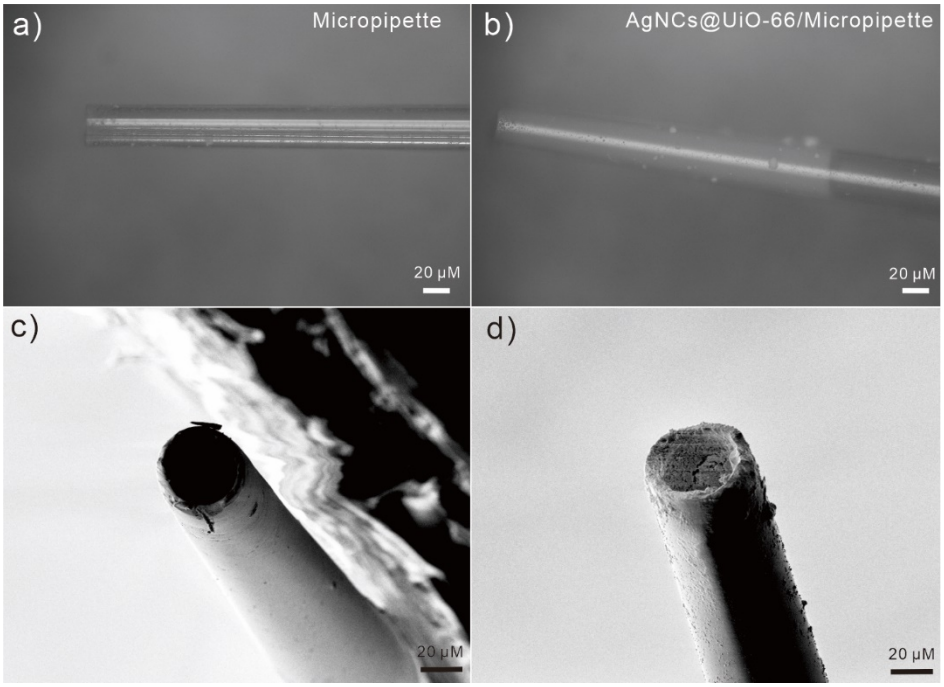

Fig. S5. (a, b) Optical images and (c, d) SEM images of (a, c) a typical micropipette and (b, d) AgNCs@UiO-66 modified micropipette.

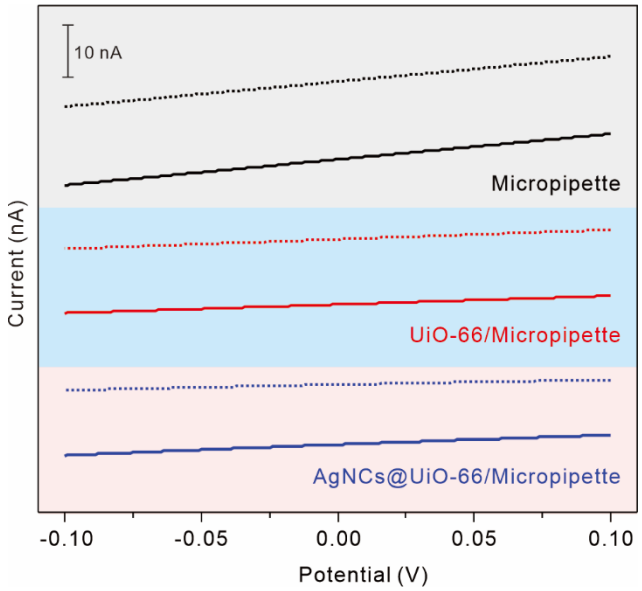

Fig. S6. The current-voltage (I-V) curves of micropipette, UiO-66(Zr) and AgNCs@UiO-66 modified micropipettes in 0.1 M NaCl in the absence (dotted line) and in the presence of 0.1 μM Na_2S (solid line) in a potential ranged between -0.1 V and +0.1 V.

Table S1. Resistance of micropipette, UiO-66(Zr)/micropipette, AgNCs@UiO-66(Zr)/micropipette measured in 0.1 M NaCl and 0.1 M NaCl containing 0.1 μM Na_2S

	Resistance (MΩ)	
	0.1 M NaCl	0.1 M NaCl + 0.1 μM Na_2S
micropipette	20.2	19.8
UiO-66(Zr)/micropipette	53.1	58.6
AgNCs@UiO-66/micropipette	95.2	49.3

The micropipette, UiO-66(Zr)/micropipette, and AgNCs@UiO-66/micropipette were characterized in in 0.1 M NaCl solution (Fig. S5). Their I-V slopes area gradually increased, that is, the corresponding resistances are increased (Table S1). Diameters of the micropipettes can be calculated electrochemically using the slope of current-voltage (I-V) curves and based on the following equation. The diameter ($2a$) at the tip of the nanopipette was calculated to be 31 ± 3 μm

$$a = \frac{1}{\pi k R \tan\frac{\theta}{2}} \quad \text{(S1)}$$

R is the measured resistance, k is the specific resistance of the electrolyte used (k = 2.5 S m^{-1} in 0.1 M NaCl), θ is the cone angle (3.1° in this case), a is the orifice radius of the nanopore at the tip of the nanopipette.

As observed, the bare micropipette exhibits the lowest resistance as 20 MΩ. While the resistance is greatly increased with the modification of UiO-66(Zr). And AgNCs@UiO-66 nanochannels lead to higher resistance. Meanwhile, in the presence of 0.1 μM Na_2S, there are no obvious change on the resistances at micropipette, UiO-66(Zr)/micropipette.

The micropipette and UiO-66(Zr)/micropipette exhibit no significant selective

response to S^{2-} upon the addition of 0.1 μM Na2S, resulting in minimal change in resistance. In contrast, as for the AgNCs@UiO-66/micropipette, increasing Na2S enhances ion flux and surface charge within the nanochannels, consequently lowering resistance.

S4. Zeta potentials of UiO-66, AgNCs@UiO-66

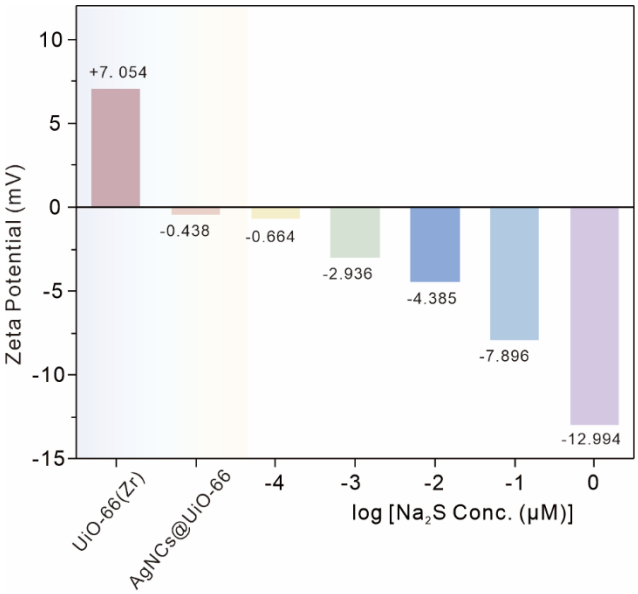

Fig. S7. Zeta potentials of UiO-66, AgNCs@UiO-66, and AgNCs@UiO-66 interacted with different concentrations of Na_2S.

S5. Interference and stability measurement

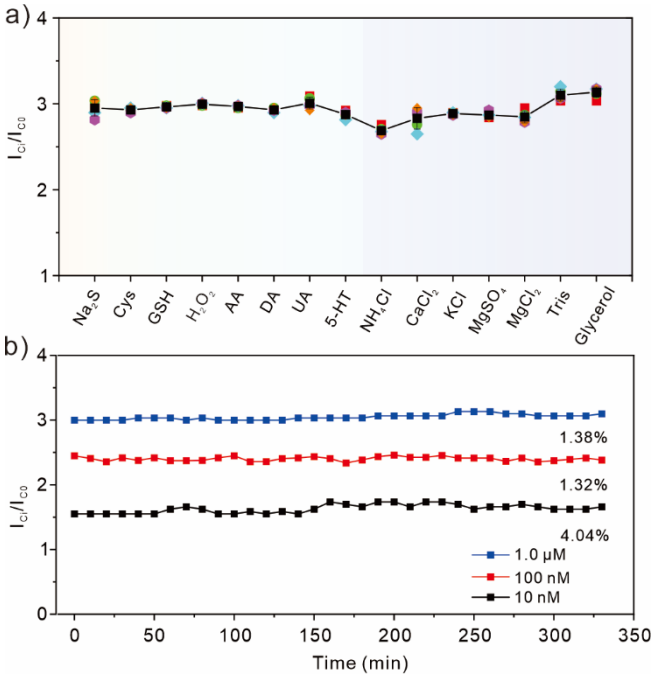

Fig. S8. (a) Interference test of AgNCs@UiO-66/micropipette toward 1.0 μM H_2S with the presence of sulfur-containing substances, other electroactive substances, and inorganic ions. (b) Stability measurements of AgNCs@UiO-66/micropipette toward Na_2S for 330 min in 0.1 M NaCl solution. Three concentrations of 10 nM, 100 nM, and 1.0 μM were tested.

As is well-known, it is susceptible to interference from electroactive species, particularly sulfur-containing species co-existed with sulfide ions, which could form an Ag−S bond and affect the sensing of Na_2S. In this work, the potential interference of AgNCs@UiO-66/micropipette is evaluated. Fig. S8a shows the current ratio of AgNCs@UiO-66/micropipette toward 1.0 μM Na_2S in the presence of the electroactive and sulfur-containing species (20 μM Cys, 20 μM GSH, 10 μM H_2O_2, 200 μM AA, 10 μM DA, 50 μM UA, 10 μM 5-HT). No obvious change in the current ratios is observed, indicating the favorable selectivity of the AgNCs@UiO-66/micropipette. The formed AgNCs@Ag_2S could be recognized as an ion-selective membrane, which could minimize the interaction of AgNCs with other sulfur-containing species, thus

avoiding interference [3]. Besides, UiO-66(Zr) nanoparticles integrated with AgNCs present the sub-nanochannels could weaken the diffusion of other electroactive species and prevents the contact of other macromolecular disruptors, thereby minimizing the interference [4,5]. Meanwhile, the surface charge within the AgNCs@UiO-66/micropipette modulates ion transport behaviors, and the interplay between the surface charge, ion mobility, and the results in electric field gradients governs the overall electrochemical dynamics, which further affect the diffusion of electroactive species. Similarly, the effect of the species that coexist in bacterial culture medium was also investigated. As observed, the current ratios of the AgNCs@UiO-66/micropipette toward 1.0 μM Na_2S are almost stable in the presence of the ingredients in bacterial culture medium (18.6 mM NH_4Cl, 90.8 mM Tris, 0.099 mM $CaCl_2$, 4.2 mM KCl, 23.1 mM $MgCl_2 \cdot 6H_2O$, 2.0 mM $MgSO_4$, 2.0 mM sodium glycerophosphate). These results indicate that the AgNCs@UiO-66/micropipette exhibits high selectivity toward Na_2S with high anti-interference capability.

Subsequently, the stability of the AgNCs@UiO-66/micropipette toward Na_2S was evaluated. The corresponding current responses are detected by I-V scanning in 0.1 M NaCl, and Fig. 4b shows the repeated current ratios at an interval of 10 min on the sensing of Na_2S in the concentrations of 0.01 μM, 0.1 μM and 1.0 μM. No remarkable changes in ratios are observed for a long-time measurement (330 min), and the relative standard deviations (RSDs) are calculated to be 4.04%, 1.32% and 1.38%, respectively. The results demonstrate that AgNCs@UiO-66/micropipette exhibits high stability in the monitoring of Na_2S.

S6. Bacterial sample measurement

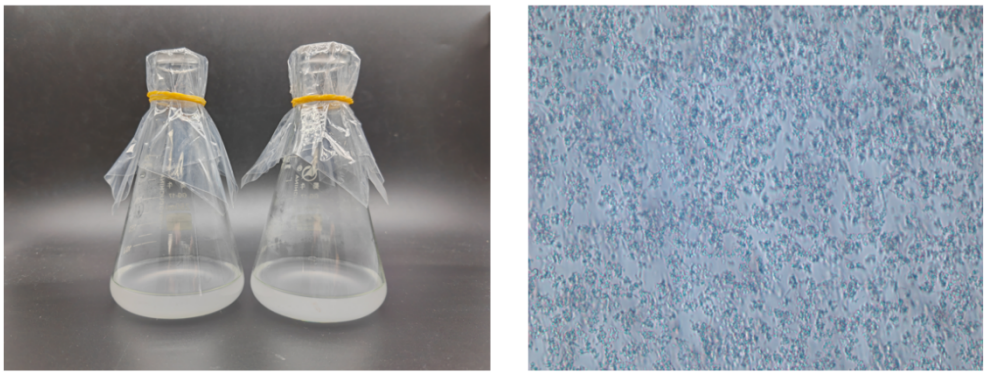

Fig. S9. Optical images of (a) bacterial culture and (b) the bacteria.

S7. A comparison in sensing performance

Table S2. A comparison of the sensing performance toward H_2S.

Material/Electrode	Method	Electrolyte + Sulfur species	Linear range (μM)	LOD (μM)	Refs
Bi-MOF-based PAD	Colorimetric		0 – 40	0.23	[6]
TPABF-HS	Fluorescence	NaHS	0 – 1000	0.42	[7]
Si/CdTe NPs	Fluorescence		1 – 20	0.3	[8]
RO-H_2S	fluorescence		0 – 150	0.37	[9]
Luc-H_2S	Fluorescence	0.01 M PBS	0 – 100	0.337	[10]
Cu[GluC]	Fluorescence	Na_2S	20 – 120	0.0496	[11]
L-Cu^{2+} Probe	Fluorescence	Na_2S	1 – 11	0.0206	[12]
FGGH-Cu	Fluorescence	NaHS		0.0222	[13]
Ti/TiO_2@HSP	Photoelectrochemistry	0.01 M PBS	0.05 – 20	0.0078	[14]
Bi/CFME microelectrode	Photoelectrochemistry	PBS + Na_2S	0 – 200	0.0074	[15]
Cu-HHTP@Zn-TCPP	Photoelectrochemistry	0.1 M Tris + Na_2S	0.1 – 1500	0.62	[16]
NH_2-UiO-66@Bi_2O_3/SWCNT film	Photoelectrochemistry	Na_2S	2.5 – 100	0.78	[17]
Ag_2S/AgNCs/CF	Electrochemistry	250 μM KCl + Na_2S	0.2 – 16.4	0.07	[18]
RuCu-HHTP/CF	Electrochemistry	0.1 M PBS	0.5 – 594400	0.5	[19]
DHP-SQR/AuNPs/LIGE	Electrochemistry	Tris-HCl buffer	0.002 – 0.1	0.0008	[20]
PB/SPE	Electrochemistry	0.1 M KCl + NaHS	10 – 100	3.0	[21]
Ag@Ag_2S core–shell NPs	Electrochemistry	0.1 M PBS + Na_2S	10 – 460 600 – 11000	4.0	[22]
$CuFe_2O_4$/Bcn/GCE	Electrochemistry	0.1 M PBS + Na_2S	0.005 – 10.0	0.00021	[23]
CoGPCs/G-FET	Electrochemistry	Na_2S	0.00001 – 1000	0.00001	[24]
CoNi-MOFs	Electrochemistry	0.1 M PBS + Na_2S	2 – 2000	1.96	[25]
AgNCs@UiO-66/ micropipette	**Electrochemistry**	**0.01 M NaCl + Na_2S**	**0.0001 – 100**	**0.0001**	**This Work**

PAD: paper analysis device; TPABF-HS: triphenylamine-benzofuran for hydrogen sulfide; RO-H_2S: 10-(diethylamino)-3-(2,4-dinitrophenoxy)-5,6-dihydrobenzo[c]xanthen-12-ium; FGGH: FITC-Gly-Gly-His-NH_2; Bcn: lotus leaf-derived carbon material; HSP: H_2S-specific probe; CFME: carbon fiber microelectrode; CF: carbon fiber; GF: DHP: Dihexadecylphosphate; SQR: quinone oxidoreductase; LIGEs: laser-induced graphene; CoGPCs: cobalt phthalocyanine RGO nanocomposites; FET: field-effect transistor

S8. References

[1] R.M. Wang, L. Liu, S. Subhan, Y. Muhammad, Y. Hu, M.Y. Huang, Y. Peng, Z.X. Zhao, Z.X. Zhao, Engineering pH-switchable UiO-66 via in-situ amino acid doping for highly selective adsorption of anionic dyes, Chem. Eng. J. 395 (2020) 124958.

[2] Y. Cao, Y.X. Zhao, Z.J. Lv, F.J. Song, Q. Zhong, Preparation and enhanced CO_2 adsorption capacity of UiO-66/graphene oxide composites, J. Ind. Eng. Chem. 27 (2015) 102-107.

[3] L. Zhang, T.C. Xu, W.L. Ji, X.F. Wang, S.W. Cheng, S. Zhang, Y. Zhang, M.N. Zhang, Ag_2S/Ag Nanoparticle Microelectrodes for In Vivo Potentiometric Measurement of Hydrogen Sulfide Dynamics in the Rat Brain, Anal. Chem. 93 (2021) 7063-7070.

[4] Z.X. Chen, L. Li, Z.S. Zhao, Y. Zhu, Z.D. Liu, Responsive luminescent silver-based metal-organic frameworks for highly sensitive and selective detection of hydrogen sulfide in biological system via a self-assembled headspace separation device, Talanta 267 (2024) 125170.

[5] Y. Zhang, H.Y. Shen, X. Hai, X.W. Chen, J.H. Wang, Polyhedral Oligomeric Silsesquioxane Polymer-Caged Silver Nanoparticle as a Smart Colorimetric Probe for the Detection of Hydrogen Sulfide, Anal. Chem. 89 (2017) 1346-1352.

[6] J.Y. Zhou, X. Gao, X.Y. Chen, H.Y. Sun, X. Li, L.Y. Shi, Y.Q. Liu, Bi-MOF-based point-of-care testing paper for dual-mode detection of H2S, Biosens. Bioelectron. 270 (2025) 116934.

[7] M.Y. Guo, X.J. Liu, Y.Z. Li, B.Z. Wang, Y.S. Yang, H.L. Zhu, A human serum albumin-binding-based fluorescent probe for monitoring hydrogen sulfide and bioimaging, Analyst 149 (2024) 1280-1288.

[8] G.B. Mao, Y. Zeng, C.M. Qiu, G.M. Ding, L.Y. Li, L.X. Ma, J.B. Dai, W. Yin, Y.X. Ma, Ratiometric fluorescent paper chip for monitoring the freshness of high protein foods, Anal. Chim. Acta 1334 (2025) 343418.

[9] X.L. Li, Y.P. Xiong, P.H. Dong, K. Zhang, B. Yan, C. Huang, T.D. James, Y.S. Li, X. Jia, Red-emitting fluorescent probe with excellent water solubility for the

in situ monitoring of endogenous H_2S in wheat under salt and Al^{3+} stress, Talanta 290 (2025) 127808.

[10] C. Hu, Z.P. Yang, X.R. Shi, Y.R. Xue, L.Y. Huang, C. Tang, F. Wang, In vivo monitoring of endogenous hydrogen sulfide and evaluation of natural protectants in liver injury mice using a highly selective bioluminescent probe, Biosens. Bioelectron. 278 (2025) 117343.

[11] X.W. An, Y. Wang, J.H. Li, Z.C. Pei, Y.X. Pei, Detection of S^{2-} in Water by a Glucose Enhanced Water-Soluble Fluorescent Bioprobe, Biosensors 12 (2022) 600.

[12] G.H. Liu, Z.L. Chai, L.L. Gan, X.X. Li, C.Y. Ma, M.X. Du, W.K. Dong, An efficient copper(II) salamo-based complex fluorescence chemosensor for detecting sulfide ions: Structure exploration and practical application, J. Mol. Struct. 1306 (2024) 137878.

[13] Y. An, L.Y. Li, L.P. Li, Y.Q. Sun, B. Li, P. Wang, Peptide-based probe for colorimetric and fluorescent detection of Cu^{2+} and S^{2-} in environmental and biological systems, J. Hazard. Mater. 465 (2024) 133192.

[14] Y.Q. Hao, Y.W. Yang, W.H. Wang, H. Gu, W.S. Chen, C.L. Li, P.S. Zhang, R.J. Zeng, M.T. Xu, S. Chen, Development of a Photoelectrochemical Microelectrode Using an Organic Probe for Monitoring Hydrogen Sulfide in Living Brains, Anal. Chem. 96 (2024) 19822-19832.

[15] Z.Y. Chen, S. Chen, W.H. Wang, W.F. Liu, H. Gu, P.S. Zhang, R.J. Zeng, Y.Q. Hao, Electrochemical in situ transformation of Bi-based photoactive materials for photoelectrochemical detection of H_2S in the living brain, Microchem. J. 211 (2025) 113164.

[16] H.L. Zhao, X.W. Li, K. Yu, H.X. Xu, Z.Y. Zhang, H.N. Chai, M.W. Tian, L.J. Qu, X.J. Zhang, G.Y. Zhang, A MOF-on-MOF based photoelectrochemical sensor for hydrogen sulfide detection in food quality assessment, Sens. Actuators B-Chem. 433 (2025) 137525.

[17] Z.P. Song, T.F. Luo, J.R. Ke, S.S. Hu, W.Q. Yang, J.C. Ni, X.P. Chen, Z.H. Chen, A new-style pohotoelectrochemical sensing device based on NH_2-UiO-

66@Bi_2O_3 for the sensitive detection of hydrogen sulfide, Microchem. J. 206 (2024) 111669.

[18] R.T. Liu, S. Zhang, H. Zeng, N. Gao, Y.Y. Yin, M.N. Zhang, L.Q. Mao, A Potentiometric Dual-Channel Microsensor Reveals that Fluctuation of H_2S is Less pH-Dependent During Spreading Depolarization in the Rat Brain, Angew. Chem. Int. Ed. 63 (2024) e202318973.

[19] Y. Xu, W. Huang, H.W. Duan, F. Xiao, Bimetal-organic framework-integrated electrochemical sensor for on-chip detection of H_2S and H_2O_2 in cancer tissues, Biosens. Bioelectron. 260 (2024) 116463.

[20] X.Z. Chen, Y. Li, Y.H. Wu, A disposable electrochemical biosensor for detection H_2S in protoplast, Microchem. J. 212 (2025) 113180.

[21] A. Glovi, A. Miglione, D.C. Maresca, F. Somma, B. Romano, A. Ianaro, A. Giordano, M. De Laurentiis, G. Ercolano, S. Cinti, Paper-based electrochemical device for the determination of H_2S in murine lysates for liquid biopsy application, Anal. Chim. Acta 1342 (2025) 343669.

[22] X.L. Liu, J.W. Dai, Z.Y. Wang, Y. Xu, A.R. Zhang, Q.Y. Lv, H.F. Liu, G.F. Li, Highly stable potentiometric sensing toward sulfide in vitro living cells with Ag@Ag_2S core-shell nanoparticles, Microchem. J. 209 (2025) 112720.

[23] N. Zou, X. Li, W.W. Xu, F.A. Meng, Z.X. Wang, J.H. Zhang, X.L. Wang, A Lower Working Potential and Real-Time H_2S Sensor Based on Nano-$CuFe_2O_4$ and Lotus Leaf Derived Carbon Material Composite, J. Electrochem. Soc. 171 (2024) 037514.

[24] L. Xiao, S.S. Yu, Q. Cui, J.C. Liu, G.W. Liang, Y.T. Li, G.J. Zhang, Phthalocyanine-functionalized field-effect transistor biosensor for in situ monitoring of cell-released hydrogen sulfide, Sens. Actuators B-Chem. 406 (2024) 135402.

[25] T. Ma, X. Liu, X.W. Wang, J.G. Ma, P. Cheng, Bottom-Up Construction of Rhombic Lamellar CoNi-MOFs for the Electrochemical Sensing of H_2S, Inorg. Chem. 63 (2024) 7504-7511.